ACCOUNTS
of chemical research

Efficient Calculation of Time- and Frequency-Resolved Four-Wave-Mixing Signals

MAXIM F. GELIN, DASSIA EGOROVA, AND
WOLFGANG DOMCKE*

Department of Chemistry, Technical University of Munich, D-85747 Garching, Germany

RECEIVED ON FEBRUARY 9, 2009

CONSPECTUS

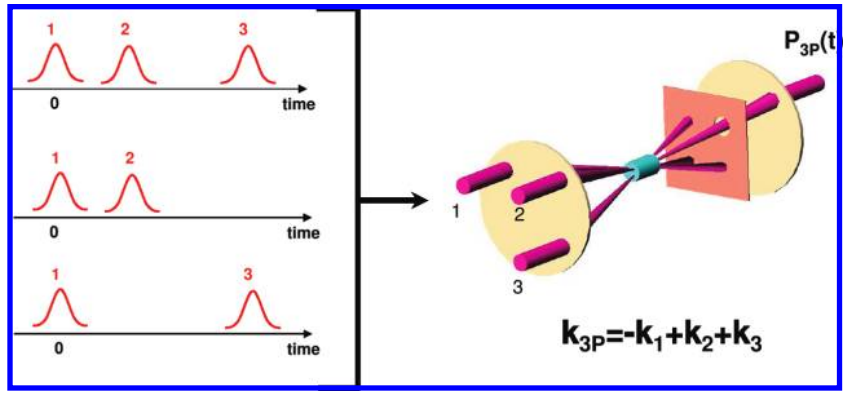

"Four-wave-mixing" is the generic name for a family of nonlinear electronic and vibrational spectroscopies. These techniques are widely used to explore dissipation, dephasing, solvation, and interstate coupling mechanisms in various material systems. Four-wave-mixing spectroscopy needs a firm theoretical support, because it delivers information on material systems indirectly, through certain transients, which are measured as functions of carrier frequencies, durations, and relative time delays of the laser pulses. The observed transients are uniquely determined by the three-pulse-induced third-order polarization.

There exist two conceptually different approaches to the calculation of the nonlinear polarization. In the standard perturbative approach to nonlinear spectroscopy, the third-order polarization is expressed in terms of the nonlinear response functions. As the material systems become more complex, the evaluation of the response functions becomes cumbersome and the calculation of the signals necessitates a number of approximations.

Herein, we review alternative methods for the calculation of four-wave-mixing signals, in which the relevant laser pulses are incorporated into the system Hamiltonian and the driven system dynamics is simulated numerically exactly. The emphasis is on the recently developed equation-of-motion phase-matching approach (EOM-PMA), which allows us to calculate the three-pulse-induced third-order polarization in any phase-matching direction by performing three (with the rotating wave approximation) or seven (without the rotating wave approximation) independent propagations of the density matrix. The EOM-PMA is limited to weak laser fields (its domain of validity is equivalent to the approach based on the third-order response functions) but allows for arbitrary pulse durations and automatically accounts for pulse-overlap effects. As an illustration, we apply the EOM-PMA to the calculation of optical three-pulse photon-echo two-dimensional (2D) signals for a generic model system, which represents a characteristic photophysical dynamics of large molecules or chromophores in condensed phases.

The EOM-PMA is easy to implement and can straightforwardly be incorporated into any computational scheme, which provides the time-dependent density matrix or wave function of the material system of interest. In particular, EOM-PMA-based computer codes can efficiently be implemented on parallel computers. The EOM-PMA facilitates considerably the computation of four-wave-mixing signals and 2D spectra, in both vibrational and electronic spectroscopy. The EOM-PMA can be extended to higher order optical responses, e.g., heterodyned 3D IR, transient 2D IR, and other six-wave-mixing techniques.

Published on the Web 05/18/2009 www.pubs.acs.org/acr
10.1021/ar900045d CCC: $71.50

1. Introduction

"Four-wave-mixing" is the generic name for a family of nonlinear multidimensional (electronic or vibrational) spectroscopies. Basically, these spectroscopies are analogues to the multidimensional nuclear magnetic resonance (NMR) techniques but use optical or infrared (rather than radio) frequencies and femtosecond (rather than millisecond) time resolution.[1,2] Four-wave-mixing spectroscopy, in particular, the three-pulse photon-echo (3PPE) technique, is a powerful tool that provides information on dissipation, dephasing, solvation, and (electronic or vibrational) interstate coupling mechanisms in various material systems.[1−10] Four-wave-mixing spectroscopy delivers information on material systems indirectly, through certain transients, which are measured as functions of carrier frequencies, durations, and relative time delays of the laser pulses. If we characterize the system dynamics in terms of the time-dependent density matrix, then four-wave-mixing spectroscopy monitors populations and coherences in real time. The monitoring of quantum coherences has become the trademark of 3PPE spectroscopy, in contrast to pump−probe and fluorescence up-conversion spectroscopies, which primarily deliver information about the (electronic or vibrational) population dynamics.

Four-wave-mixing spectroscopy is an intrinsically nonlinear technique. The observed transients are uniquely determined by the three-pulse-induced third-order polarization. Rephrasing Feynman,[11] the nonlinear polarization is the summit of four-wave-mixing spectroscopy. The entire subject is either the climb up to the summit (when we calculate the nonlinear polarization) or the slide down from the summit (when the nonlinear polarization is used to calculate four-wave-mixing signals).

There exist two major techniques for the climb up to the summit. In the standard perturbative approach, the third-order polarization $P(t)$ is expressed as a triple time integral involving the nonlinear response function[3]

$$\int_0^\infty dt_1 \int_0^\infty dt_2 \int_0^\infty dt_3 S(t_1, t_2, t_3) E(t - t_3) E(t - t_3 - t_2) \times E(t - t_3 - t_2 - t_1) \quad (1)$$

Here, $E(t)$ represents the electric field of the three pulses involved and parametrically depends upon their carrier frequencies, phases, and mutual delays. The nonlinear response function $S(t_1, t_2, t_3)$ is determined by the dynamics of the material system in the absence of external pulses. It can be calculated analytically for few-level systems or (damped) harmonic oscillator systems.[3] As the material systems become more complex and their dynamics becomes nonlinear, the evaluation of the response functions necessitates a number of approximations[8,9,12] or requires extensive computer simulations.[13,14] The nonlinear response functions can also be calculated through the time-evolution equations for the density matrix of the material system.[15] These advanced approaches to the evaluation of nonlinear response functions are reviewed by Tanimura and Ishizaki in this special issue.

The conceptual alternative to the perturbative approach (eq 1) is the nonperturbative evaluation of time- and frequency-resolved spectra. All relevant optical fields $E(t)$ are incorporated into the system Hamiltonian, and the dynamics of the driven system is calculated numerically exactly. The present paper reviews such nonperturbative approaches to the calculation of four-wave-mixing signals. The structure of the paper is inspired by Feynman's mountaineering allegory mentioned above. Section 2 gives a short overview of the existing nonperturbative methods. The emphasis is on the recently developed equation-of-motion phase-matching approach (EOM-PMA).[16,17] Section 3 illustrates applications of the EOM-PMA to the calculation of optical 3PPE two-dimensional (2D) signals for a generic model system, which represents characteristic photophysical dynamics in large molecules and condensed phases, accounting for strong electronic and electronic−vibrational coupling effects. It also includes vibrational relaxation and dephasing via the coupling of the reaction mode to a thermal environment. Section 4 contains conclusions and an outlook.

2. Climb Up to the Summit: Calculation of the Nonlinear Polarization

2.1. Nonperturbative Methods for the Calculation of Four-Wave-Mixing Signals. The idea behind the nonperturbative approach is simple and obvious. For the study of the dynamics of the vast majority of chemically interesting systems, we have to resort to numerical methods and/or simulations. Suppose that we wish to calculate the spectroscopic response of such a system. To do so, we have to take into account the interaction of the system with the pertinent laser pulses. Because we have to resort to a numerical simulation anyway, it seems logical to incorporate all relevant laser fields into the system Hamiltonian (which thus becomes time-dependent) and to calculate numerically the dynamics of the driven system.[18] Because no assumptions are made about the relative timings of the pulses involved, all effects because of pulse overlaps are accounted for automatically. This is the great advantage of the nonperturbative approach. When dealing with complex multilevel systems (notably with strong electronic and vibrational couplings as well as with bath-induced relaxations),

the nonperturbative approach has proven its advantage over perturbative treatments.[18] The nonperturbative approach has been applied to various time- and frequency-resolved two-pulse (see ref 19 for a recent review) and three-pulse[16,17,20−28] spectroscopic techniques.

In the nonperturbative approach, we have to pay a certain overhead, however. The problem is that a nonperturbative calculation yields the total polarization, which must be further decomposed to single out a specific combination of the wave vectors (the so-called phase-matching condition) characteristic for a particular optical signal. The problem can be resolved be performing a discrete Fourier transform of the underlying Liouville equation with respect to the phases of the pertinent pulses.[5,6] Alternatively, we can compute the total polarization for different phases of the pulses involved and express the polarization for a certain phase-matching condition as a linear combination of the computed total polarizations. For two-pulse techniques, this requires four independent calculations of the total polarization.[18] For the calculation of four-wave-mixing signals, the situation is more involved. As shown in refs 20−22, the extraction of the 3PPE polarization from the total polarization within the rotating wave approximation (RWA) requires the solution of a 12×12 system of linear equations. This implies that one has to determine the time evolution of 12 density matrices (in fact, one has to perform three additional time propagations to remove the linear terms from the nonlinear polarization) and to solve a 12×12 system of linear matrix equations at each time step. Without invoking the RWA, the computational cost is even higher.

The EOM-PMA leads to a substantial simplification of these calculations. This method, which has been developed in refs 16 and 17 for systems with strong electronic−vibrational couplings and extended in ref 24 to multichromophoric systems with static disorder, is outlined below in a general form, which is equally suitable for electronic and vibrational spectroscopy.

2.2. EOM-PMA. Let H be the system Hamiltonian. The system−field interaction in the dipole approximation is written as

$$H_{\text{int}}(t) = -\sum_{a=1}^{3} (\exp\{+i\mathbf{k}_a\mathbf{r}\}v_a^{(+)}(t) + \exp\{-i\mathbf{k}_a\mathbf{r}\}v_a^{(-)}(t)) \quad (2)$$

$$v_a^{(\pm)}(t) = V\lambda_a E_a(t - \tau_a)\exp\{\mp i\omega_a t\} \quad (3)$$

Here, λ_a, $\mathbf{k}_a$, ω_a, $E_a(t)$, and τ_a denote the intensity, wave vector, frequency, dimensionless envelope, and the central time of the pulses; V is the transition-dipole-moment operator. We can thus write the master equation for the reduced density matrix ($\hbar = 1$)

$$\partial_t\rho(t) = -i[H + H_{\text{int}}(t), \rho(t)] + D\rho(t) \quad (4)$$

with D being a suitable dissipative operator.[29,30] For simplicity of notation, D is written as a time-independent operator. Upon the substitution $D\rho(t) \rightarrow \int_0^t dt' D(t - t')\rho(t')$, all the derived formulas remain true for a general non-Markovian dissipative operator. Strictly speaking, D depends upon the laser fields involved. Because we consider weak laser pulses, this effect can safely be neglected.[31] If we include all of the relevant degrees of freedom into the system Hamiltonian H, then, of course, $D = 0$.

The total laser-induced polarization is

$$P(t) \equiv \langle V\rho(t)\rangle \quad (5)$$

where the angular brackets indicate the trace. We wish to extract the 3PPE polarization $P_{3P}(t)$ from eq 5; that is, we search for the contribution that is proportional to $\exp\{\pm i\mathbf{k}_{3P}\mathbf{r}\}$ and thus obeys the 3PPE phase-matching condition

$$\mathbf{k}_{3P} = -\mathbf{k}_1 + \mathbf{k}_2 + \mathbf{k}_3 \quad (6)$$

so that

$$P_{3P}(t) = P_{3P}^{(+)}(t)\exp\{+i\mathbf{k}_{3P}\mathbf{r}\} + c.c. \quad (7)$$

It is thus sufficient to evaluate the complex polarization $P_{3P}^{(+)}(t)$. For this purpose, only terms with the phase factors $\exp\{-i\mathbf{k}_1\mathbf{r}\}$, $\exp\{+i\mathbf{k}_2\mathbf{r}\}$, and $\exp\{+i\mathbf{k}_3\mathbf{r}\}$ can be retained in the Hamiltonian interaction (eq 2). The master equation obtained in this manner

$$\partial_t\rho_1(t) = -i[H + v_1^{(-)}(t) + v_2^{(+)}(t) + v_3^{(+)}(t), \rho_1(t)] + D\rho(t) \quad (8)$$

and the original master eq 4 yield exactly the same complex polarization $P_{3P}^{(+)}(t)$. Equation 8 contains, however, only half of the Liouville pathways contributing to eq 4, which facilitates the extraction of $P_{3P}^{(+)}(t)$. Indeed, let us consider $\rho_1(t)$ in eq 8 as a function of the pulse strengths

$$\rho_1(\lambda_1, \lambda_2, \lambda_3; t) = \sum_{i,j,k=0}^{\infty} \lambda_1^i\lambda_2^j\lambda_3^k\rho_1^{i,j,k}(t) \quad (9)$$

$\rho_1(\lambda_1, \lambda_2, \lambda_3; t)$ can be regarded as a generating function for the various Liouville pathways, which allows us to compute a particular contribution to the total polarization, obeying the necessary phase-matching condition. In our case

$$P_{3P}^{(+)}(t) = \exp\{i\mathbf{k}_{3P}\mathbf{r}\}\langle V\rho_1^{111}(t)\rangle \quad (10)$$

As can be proven by expanding $\rho_1(\lambda_1, \lambda_2, \lambda_3; t)$ in a Taylor series

$$\lambda_1\lambda_2\lambda_3\rho_1^{111}(t) = \rho_1(\lambda_1, \lambda_2, \lambda_3; t) + \rho_1(\lambda_1, 0, 0; t) - \rho_1(\lambda_1, 0, \lambda_3; t) - \rho_1(\lambda_1, \lambda_2, 0; t) - \rho_1(0, \lambda_2, \lambda_3; t) - \rho_1(0, 0, 0; t) + \rho_1(0, 0, \lambda_3; t) + \rho_1(0, \lambda_2, 0; t) + O(\lambda_1^n\lambda_2^k\lambda_3^m),\ n + k + m > 3 \quad (11)$$

Therefore, the 3PPE polarization can be evaluated as

$$P_{3P}^{(+)}(t) = \exp\{i\mathbf{k}_{3P}\mathbf{r}\}\langle V(\rho_1(t) - \rho_2(t) - \rho_3(t) + \rho_4(t) - \hat{\rho}_1(t) + \hat{\rho}_2(t) + \hat{\rho}_3(t))\rangle \quad (12)$$

Here, $\rho_1(t)$ obeys eq 8 and

$$\partial_t\rho_2(t) = -i[H + v_1^{(-)}(t) + v_2^{(+)}(t), \rho_2(t)] + D\rho_2(t) \quad (13)$$

$$\partial_t\rho_3(t) = -i[H + v_1^{(-)}(t) + v_3^{(+)}(t), \rho_3(t)] + D\rho_3(t) \quad (14)$$

$$\partial_t\rho_4(t) = -i[H + v_1^{(-)}(t), \rho_4(t)] + D\rho_4(t) \quad (15)$$

The density matrices $\hat{\rho}_i(t)$ obey the same equations as the corresponding density matrices $\rho_i(t)$ but with the $v_1^{(-)}(t)$ term omitted. In writing eq 12, we have used the fact that $\langle V\rho_1(0, 0, 0; t)\rangle \equiv 0$, assuming that there exists no permanent dipole moment in the ground state.

A few comments are in order. First, the $\rho_i(t)$ and $\hat{\rho}_i(t)$ are not true density matrixes. Because the $v_a^{(\pm)}(t)$ functions are complex, $\rho_i(t)$ and $\hat{\rho}_i(t)$ are not Hermitian operators. Second, eq 12 is valid in the leading order of the perturbation expansion in the optical fields involved; that is, $P_{3P}(t) \sim \lambda_1\lambda_2\lambda_3 + O(\lambda_1^n\lambda_2^k\lambda_3^m)$, where $n + k + m > 3$. Thus, the domain of validity of eq 12 coincides with that of the third-order perturbation expansion (eq 1). Third, eq 12 accounts for all effects because of pulse overlaps automatically.

Static inhomogeneous broadening of the 3PPE transients has to be taken into account in many practically important cases. Because of the interaction with an environment, the frequencies of the electronic transitions are not fixed but have a certain distribution. Therefore, we have to average the 3PPE signals over this distribution. This procedure can efficiently be accomplished by the method suggested in ref 24.

Summarizing, to calculate the time evolution of the 3PPE polarization for particular values of the pulse delay times, we have to perform seven density-matrix propagations. It is important to note that not all seven equations depend upon the central times of the pulses simultaneously, which allows for considerable simplifications and optimizations in the computation of 3PPE signals. All other four-wave-mixing signals can be calculated in an analogous manner.

2.3. Rotating Wave Approximation. The EOM-PMA scheme of the calculation of the 3PPE polarization presented in section 2.2 is general. It is valid for any system interacting with three transform-limited laser pulses. The EOM-PMA can further be simplified by invoking the RWA to the system−field Hamiltonian interaction.

Let ε_α be the eigenenergies of the system Hamiltonian

$$H|\alpha\rangle = \varepsilon_\alpha|\alpha\rangle,\ \varepsilon_0 < \varepsilon_1 < \varepsilon_2 \ldots \quad (16)$$

The RWA amounts to the omission of the counter-rotating terms ($\sim\exp\{\pm i(\varepsilon_\alpha + \omega_a)t\}$) while retaining the co-rotating terms ($\sim\exp\{\pm i(\varepsilon_\alpha - \omega_a)t\}$) in the master equation (eq 4). The use of the RWA is justified if the phase factors $\exp\{\pm i(\varepsilon_\alpha + \omega_a)t\}$ are highly oscillatory on the time scale of the system dynamics. It is well-established that the RWA is accurate for electronic spectroscopy with visible or UV pulses. It can also be applied in infrared spectroscopy if there exists a clear separation of high- and low-frequency vibrational modes.

Within the RWA, the interaction Hamiltonian (eq 2) can be written as follows:

$$H_{\text{int}}(t) = -\sum_{a=1}^{3}(\exp\{+i\mathbf{k}_a\mathbf{r}\}v_a^{>}(t) + \exp\{-i\mathbf{k}_a\mathbf{r}\}v_a^{<}(t)) \quad (17)$$

$$v_a^{>}(t) = V_{>}\lambda_a E_a(t - \tau_a)\exp\{-i\omega_a t\},$$
$$v_a^{<}(t) = V_{<}\lambda_a E_a(t - \tau_a)\exp\{i\omega_a t\} \quad (18)$$

Here, $V_>$ and $V_<$ are so-called up and down transition dipole moments. In the eigenvalue representation of the system Hamiltonian (eq 16)

$$(V_{>})_{\alpha\beta} = \begin{cases} V_{\alpha\beta} \text{ for } \alpha > \beta \\ 0 \text{ for } \alpha \le \beta \end{cases},\ (V_{<})_{\alpha\beta} = \begin{cases} V_{\alpha\beta} \text{ for } \alpha < \beta \\ 0 \text{ for } \alpha \ge \beta \end{cases},$$
$$V_{\alpha\beta} \equiv \langle\alpha|V|\beta\rangle \quad (19)$$

Clearly, all of the expressions derived in section 2.2 remain valid within the RWA, provided that we replace $v_a^{(-)}(t)$ by $v_a^{<}(t)$ and $v_a^{(+)}(t)$ by $v_a^{>}(t)$.

The RWA leads to a substantial simplification of the key formulas (eqs 12−15). Consider, for example, a system with a ground state ($|g\rangle$) and an excited electronic state ($|e\rangle$), which may be coupled to any number of vibrational modes q. Then

$$V_{>} = X^\dagger V(q),\ V_{<} = XV(q);\ X^\dagger \equiv |e\rangle\langle g|,\ X \equiv |g\rangle\langle e| \quad (20)$$

Here, the matrix element of the transition dipole moment $V(q)$ may depend upon the vibrational coordinates q because of non-Condon effects. Evidently, the X matrices obey the properties

$$(X^\dagger)^2 \equiv X^2 \equiv 0;\ X^\dagger X \equiv |e\rangle\langle e|,\ XX^\dagger \equiv |g\rangle\langle g| \quad (21)$$

Because of the identities of eq 21, $\langle X\rho_4(t)\rangle \equiv 0$. Furthermore, $\langle X\hat{\rho}_1(t)\rangle = \langle X(\hat{\rho}_2(t) + \hat{\rho}_3(t))\rangle$, because only the terms linear in the

laser pulses contribute to $\hat{\rho}_1(t)$, $\hat{\rho}_2(t)$, and $\hat{\rho}_3(t)$. The last three terms in eq 12 cancel each other, and we arrive at the result[16,17]

$$P_{3P}^{(+)}(t) = \langle X(\rho_1(t) - \rho_2(t) - \rho_3(t))\rangle \quad (22)$$

The 3PPE polarization for any electronic two-level system can thus be evaluated within the RWA by performing propagations of only three density matrices. The analysis can straightforwardly be generalized to systems with more than two electronic levels.

3. Slide Down from the Summit: Application of the EOM-PMA to 2D Electronic Three-Pulse Photon Echo Spectroscopy

To illustrate the application of the EOM-PMA, we consider a model system with a nontrivial multilevel excited-state dynamics. The system dynamics is governed by electronic interstate couplings, electron-vibrational intrastate interactions, as well as weak dissipation induced by the interaction with a harmonic bath. We calculate 2D electronic 3PPE spectra for this model to show how the signals reflect the underlying system dynamics by the comparison of the signals to characteristic system observables, such as excited electronic-state populations and expectation values of the nuclear coordinate.

3.1. Model Hamiltonian, Relaxation Operators, and Observables. The system is described by a single dimensionless coordinate Q coupled to three (one ground $|g\rangle$ and two excited $|e1\rangle$ and $|e2\rangle$) electronic states. Adopting a diabatic electronic representation and the harmonic approximation, the system Hamiltonian reads

$$H = H_g + H_e \quad (23)$$

$$H_g = |g\rangle h_g \langle g| \quad (24)$$

$$H_e = |e1\rangle(h_{e1} + \varepsilon_1)\langle e1| + |e2\rangle(h_{e2} + \varepsilon_2)\langle e2| + (V_{12}|e1\rangle\langle e2| + h.c.) \quad (25)$$

$$h_i = \frac{\Omega}{2}\{P^2 + Q^2\} - \Omega\Delta_i Q \quad (26)$$

where $i = g$, $e1$, and $e2$. P is the momentum conjugated to the coordinate Q, and $\Omega = 0.074$ eV ($\approx$600 cm^{-1}) is the vibrational frequency of the harmonic mode. $\Delta_1 = 1$ and $\Delta_2 = 3$ are the dimensionless displacements of the excited-state equilibrium geometry from that of the ground state ($\Delta_g = 0$). The vertical excitation energies are chosen as $\varepsilon_2 = \varepsilon_1 + 2\Omega$, and the electronic coupling $V_{12} = 0.02$ eV. The corresponding diabatic and adiabatic potential energy surfaces are shown in Figure 1.

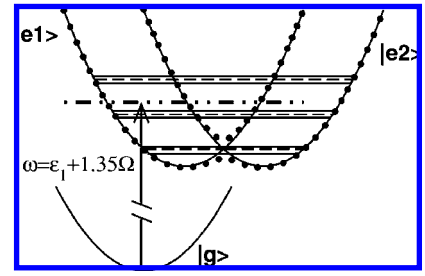

FIGURE 1. Electronic ground state (solid line), excited-state diabatic (solid lines) and adiabatic (dots) potential energy surfaces for our model system. Unperturbed vibrational levels (dashed lines) and vibronic eigenstates (solid lines), as well as the pulse carrier frequency are indicated.

All of the laser pulses involved are assumed to have Gaussian envelopes

$$E(t) = \exp\{-(\Gamma t)^2\} \quad (27)$$

equal amplitudes, the same carrier frequencies ($\omega_1 = \omega_2 = \omega_3 = \omega = \varepsilon_1 + 1.35\Omega$), and durations (full width at half-maximum $2(\ln 2)^{-1/2}/\Gamma = 25$ fs). It is assumed that the excited state $|e1\rangle$ is optically bright, while the state $|e2\rangle$ is optically dark. The operator X in eqs 20−22 is thus defined as

$$X = |g\rangle\langle e1| \quad (28)$$

The Condon approximation is used, so that $V(q) = 1$ in eq 20.

The relaxation operator D in eqs 8, 13, and 14 is taken as the sum of the vibrational relaxation operator $\mathscr{R}$ and the optical dephasing operator $\not{p}$

$$D\rho_i(t) = \mathscr{R}\rho_i(t) + \not{p}\rho_i(t) \quad (29)$$

where $\mathscr{R}$ is described by multilevel Redfield theory, as detailed elsewhere[16,17,27,28] (see also ref 32). Briefly, vibrational relaxation is introduced via a bilinear coupling of the system oscillator mode to a harmonic bath, characterized by an Ohmic spectral function $J(\omega_b) = \omega\eta_b\exp(-\omega_b/\omega_c)$,[29] where η is a dimensionless system−bath coupling parameter and ω_c is the bath cutoff frequency. The optical dephasing operator is defined as

$$\not{p}\rho(t) \equiv \xi_{eg}P_g\rho(t)P_e + h.c. \quad (30)$$

with ξ_{eg} being the optical dephasing rate, $P_g \equiv |g\rangle\langle g|$ being the projector to the ground electronic state, and $P_e \equiv 1 - P_g$. The vibrational relaxation parameters are chosen as $\eta = 0.1$, $\omega_c = \Omega$, and the optical dephasing rate $\xi_{eg} = 130$ fs^{-1} ($\sim$0.07Ω), which is reasonable for the low temperature (10 K) considered.

The 3PPE polarization $P_{3P}(t)$ is calculated within the RWA via eq 22. In addition to the 3PPE 2D spectra, we monitor characteristic system observables, such as the diabatic population of the state $|e1\rangle$

$$P_1(t) = \langle e1|\rho(t)|e1\rangle \tag{31}$$

and the expectation value of the system vibrational coordinate in the excited state

$$Q_e(t) = \langle e|\rho(t)Q|e\rangle/\langle e|\rho(t)|e\rangle \tag{32}$$

where $|e\rangle = |e1\rangle \otimes |e2\rangle$. The density matrix $\rho(t)$ in eqs 31 and 32 is calculated according to the standard Redfield equation [the relaxation operator is defined by eq 29 with $\rho_i(t) = \rho(t)$], and the interaction with the pump field is included in the commutator. The pump-pulse amplitude, frequency, and duration for the calculation of $P_1(t)$ and $Q_e(t)$ are as those of the pulses in the 3PPE setup. The pump pulse is centered at $t = 0$.

3.2. Two-Dimensional Three-Pulse Photon Echo. The 2D 3PPE signal is determined by two Fourier transformations of the nonlinear polarization $P_{3P}(t, \tau, T)$ with respect to the coherence time τ (delay between the first two pulses) and the detection time t

$$I(\omega_\tau, \omega_t, T) \sim \int d\tau \int dt \exp(-i\omega_\tau\tau)\exp(i\omega_t t)P_{3P}(t, \tau, T) \tag{33}$$

where T is the population time, i.e., the delay between the second and third pulses. The frequencies associated with the coherence time, ω_τ, and the detection time, ω_t, are usually referred to as absorption (or excitation) and emission (or probe) frequencies, respectively. The two dimensions are provided by ω_τ and ω_t, and the 2D scans are recorded at a fixed population time T. The 2D signal (eq 33) is complex-valued. Here, we consider only the real part, which is associated with the absorptive changes.[1] The displayed emission and absorption frequencies (ω_t and ω_τ) are given relative to the vertical excitation energy ε_1. The latter is arbitrary and does not need to be explicitly defined.

Figure 2 shows 2D scans calculated for various population times. The absorption frequency ω_τ reveals those system transitions that are excited in the experiment. The emission frequency ω_t, on the other hand, indicates at which frequencies the emission takes place. On the diagonal of each 2D scan, the peaks corresponding to $\omega_\tau = \omega_t$ are located, whereas the peaks with $\omega_\tau \neq \omega_t$ are the so-called cross-peaks. Within the employed resolution conditions (low temperature and short pulses), the obtained 2D spectra reveal the multilevel structure of the electronic states to a good extent. The most strongly populated levels are those closest to the laser frequency and correspond to $\omega_\tau = 0.067$ and 0.082 eV. The transitions to the levels that are about one vibrational quantum higher and lower than the most efficiently populated levels are also resolved. All of the excited levels are optically coupled to the ground-state vibrational manifold. Therefore, there are many ways to satisfy $\omega_\tau \neq \omega_t$. The ground-state manifold is harmonic, and the location of the peaks in the 2D patterns reveals the system frequencies in the excited state (cf. Figure 1). The larger splittings between the peaks are of the order of the vibrational frequency Ω. The smaller splittings arise because of the interstate electronic coupling V_{12}.

A comparison of the 2D scans for various population times reveals considerable intensity modulations of the peaks. There are several mechanisms leading to these intensity modulations. One of them is population relaxation: while absorption occurs always at the same frequencies (if the pulse parameters remain unchanged), emission depends upon T because of the population flow from higher to lower levels. At larger T, the 2D pattern may thus loose some intensity in the region of larger ω_t and gain intensity at smaller emission frequencies. Another reason for the signal intensity modulations with T are coherences, which can be created during the excitation process. If several levels are coherently excited, signal modulations with frequencies corresponding to energy differences between these levels can occur. The intensity modulations in Figure 2 are rather of the coherent character, while the effect of population relaxation is not yet very prominent at the short population times considered. The two dominant time scales of oscillations in the peak intensities are determined by the characteristic system frequencies, i.e., by the vibrational frequency Ω (higher frequency) and by the electronic coupling V_{12} (lower frequency). The faster time scale is revealed, e.g., by comparison of the scans at $T = 0$, 30, and 60 fs. The off-diagonal peaks lose their intensity at 30 fs and reappear again at 60 fs. The longer period is visible, e.g., as a pronounced change in the structure of the central peak at $T = 140$ fs, compared to $T = 0$, 30, or 60 fs. At early times (upper panels in Figure 2), one can clearly see a four-peak substructure, whereas at 140 fs, essentially one peak is resolved.

A better view of the oscillations of peak intensities with T is provided by Figure 3, which shows the intensity modulation of the cross (Figure 3a) and diagonal (Figure 3b) peaks. The excited-state coordinate expectation value $Q_e(t)$ is depicted in Figure 3c. The low-frequency oscillations in the peak intensities are suppressed relatively quickly. Essentially, a single beating at $T \approx 300$ fs (Figure 3a) and $T \approx 250$ fs (Figure 3b) is resolved. The high-frequency beatings in the peak intensities and in $Q_e(t)$ survive for longer times. The cross-peak intensity evolution (solid line in Figure 3a) and the population dynamics $P_1(t)$ (dashed line in Figure 3a) contain very similar information. The low-frequency oscillations are in phase, are modulated by higher frequencies and decay on the same

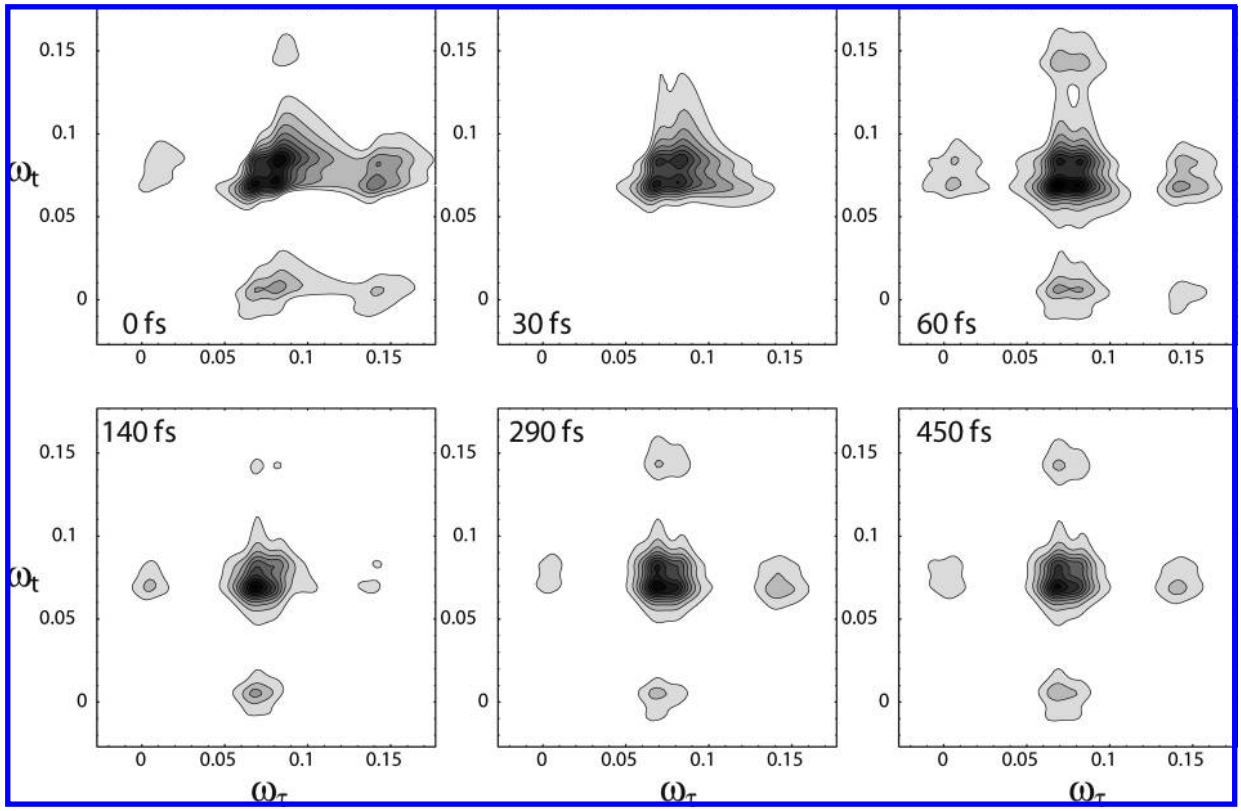

FIGURE 2. Two-dimensional 3PPE scans for different population times (indicated on the panels). The intensity scaling is the same in all graphs. Only positive parts of the spectra are displayed.

time scale. In addition to the oscillations, the diagonal-peak intensity (Figure 3b) exhibits a slow decay, which reflects population relaxation to lower states. The coordinate expectation value (Figure 3c) shows the oscillations between the two diabatic electronic states and the subsequent relaxation to the value $\langle Q \rangle = 2$, which corresponds to the mean value of the minima at $Q = 1$ and 3.

4. Conclusions and Outlook

We have reviewed a novel and efficient method for the calculation of the three-pulse-induced third-order polarization. In this method, the interactions of the system with the relevant laser pulses are incorporated into the system Hamiltonian and the driven system dynamics is simulated numerically exactly. We have described in some detail the EOM-PMA, which allows for the calculation of the third-order polarization in any phase-matching direction by performing three (with the RWA) or seven (without the RWA) *independent* propagations of the density matrix. As has been pointed out in ref 24, the EOM-PMA-based computer codes can therefore efficiently be implemented on parallel computers. The EOM-PMA is limited to weak laser fields (its domain of validity is equivalent to the approach based on the third-oder response functions) but allows for arbitrary pulse durations and automatically accounts for pulse-overlap effects.

The EOM-PMA can straightforwardly be incorporated into any computer program, which provides the time evolution of the density matrix or the wave function of any material system of interest. Besides the multilevel Redfield equation[16,17,27,28] and the non-Markovian time-nonlocal master equation,[24−26] the EOM-PMA can be combined with the Lindblad master equation,[33] the surrogate Hamiltonian approach,[33] the stochastic Liouville equation,[30] the quantum Fokker−Planck equation,[30] and the density matrix[34] or the wave function[19] multiconfigurational time-dependent Hartree (MCTDH) methods.

Nonperturbative methods have also been applied to calculate two-time fifth-order nonresonant Raman response functions,[35−37] three-time third-order infrared response functions,[38,39] and (within additional approximations) three-time third-order optical response functions[40] via classical non-equilibrium molecular dynamics simulations. Note that the method by Yagasaki and Saito[38] (see their eq 6) is conceptually similar to the EOM-PMA. We propose that the EOM-PMA can also be incorporated into non-equilibrium computer simulation schemes. The application of this strategy for optical

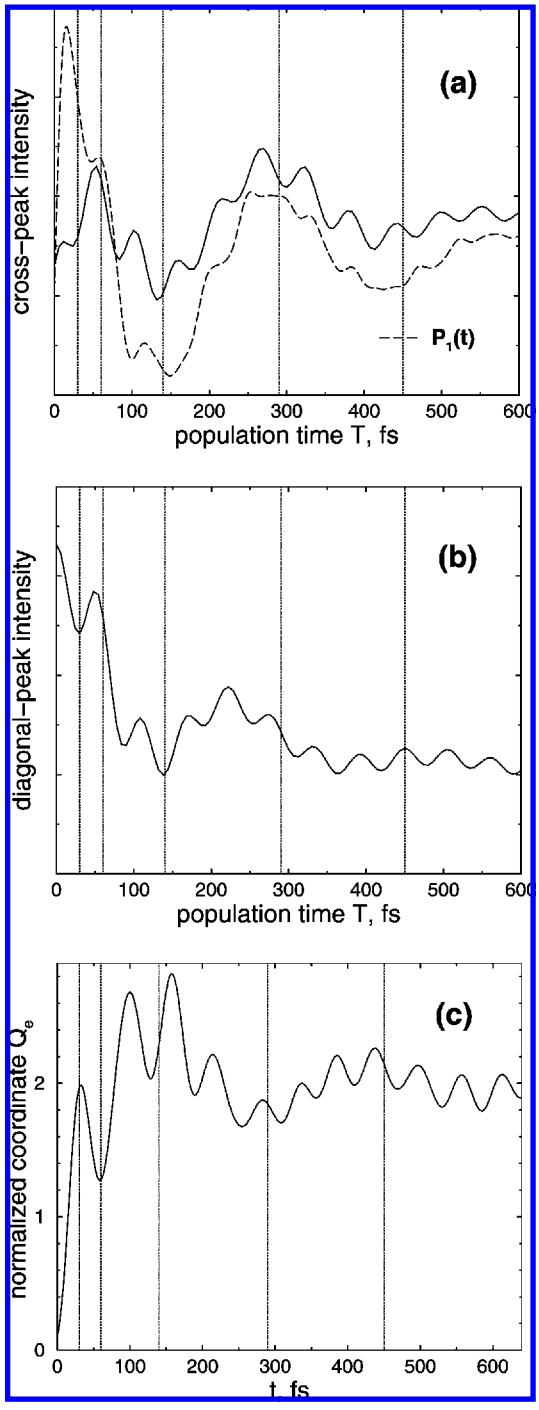

FIGURE 3. Intensities of the cross-peak at $\omega_\tau = 0.067$ eV and $\omega_t = 0.082$ eV (a) and diagonal peak at $\omega_\tau = \omega_t = 0.082$ eV (b) versus the population time T. The dashed line in panel a depicts the population dynamics $P_1(t)$ of the diabatic state $|e1\rangle$. (c) Excited-state expectation value of the coordinate $Q_e(t)$ versus t. The vertical lines indicate T at which 2D spectra in Figure 2 are shown.

four-wave mixing signals may require additional approximations, e.g., similar to those made in ref 40. The application of the EOM-PMA to infrared signals, on the other hand, seems to be quite straightforward. One can thus avoid the problem of computing stability matrices, which is a bottleneck in semiclassical simulations of the response functions.[13] Of course, we have to perform three (with the RWA) or seven (without the RWA) series of (short) molecular dynamics simulations (with the initial conditions sampled according to the equilibrium distribution without pulses) to obtain the four-wave-mixing signal for particular values of interpulse delays and carrier frequencies. To obtain the signal for different values of the parameters, the simulation cycle must be repeated, which can be computationally expensive. Nevertheless, this procedure can be much cheaper than the direct simulation of the nonlinear response functions and subsequent calculation of signals by multiple time integrals (eq 1). If we are interested, e.g., in a four-wave-mixing transient as a function of the delay T between the second and third pulses, we can obtain the desired signal by performing $3N$ (with the RWA) or $7N$ (without the RWA) series of simulations, with N being the number of discretization intervals on the T axis. On the other hand, the complete three-time response function $S(t_1, t_2, t_3)$ is necessary for the calculation of any particular four-wave-mixing transient beyond the impulsive limit. This approach requires $\sim N_1 \times N_2 \times N_3$ series of simulations and N subsequent evaluations of triple time integrals.

To summarize, we propose that the EOM-PMA can considerably facilitate the computation or simulation of various four-wave-mixing signals and 2D spectra in the visible as well as infrared spectral regions. The formalism can be extended to higher order optical responses, e.g., heterodyned 3D IR,[41,42] transient 2D IR,[7] polarizability response spectroscopy,[43] or interference between four- and six-wave-mixing signals.[44]

This work has been supported by the Deutsche Forschungsgemeinschaft (DFG) through a research grant and through the DFG Cluster of Excellence "Munich Centre of Advanced Photonics" (www.munich-photonics.de).

BIOGRAPHICAL INFORMATION

Maxim Gelin received his diploma in theoretical physics in 1988 from the Belorussian State University (Minsk) and his Ph.D. degree in theoretical optics in 1995 from the Institute of Molecular and Atomic Physics (Minsk, Belarus). His research interests are in theoretical nonlinear spectroscopy, rotational relaxation phenomena in the gas and condensed phases, and non-equilibrium statistical mechanics.

Dassia Egorova received her diploma in physics in 1998 from the State Pedagogical University of Russia (St. Petersburg) and her Ph.D. degree in theoretical chemistry in 2003 from the Technical University of Munich (Germany). Her research focuses on dissipative quantum dynamics of complex systems, in particular, simulations of time- and frequency-resolved nonlinear spectra. She is particularly interested in the capabilities of var-

ious femtosecond spectroscopic techniques to provide unambigous information on the underlying ultrafast dynamics.

Wolfgang Domcke received his diploma and Ph.D. degrees in physics from the Technical University of Munich (TUM) in 1973 and 1975, respectively. Having received the habilitation degree in 1979 from the University of Freiburg, he moved on to become Associate Professor of Theoretical Chemistry at the University of Heidelberg and later at the TUM. In 1996, he became Full Professor at the University of Düsseldorf. In 1999, he returned to the TUM, where he currently is the holder of the Chair of Theoretical Chemistry. His research interests comprise the application of electronic-structure theory for the calculation of excited-state potential-energy surfaces of polyatomic molecules, the theoretical description of non-adiabatic dynamics in photochemistry, vibronic-coupling effects in molecular spectroscopy, and the theory of nonlinear time-resolved spectroscopy of polyatomic molecules.

FOOTNOTES

*To whom correspondence should be addressed. Fax: +49-89-289-13622. E-mail: wolfgang.domcke@ch.tum.de.

REFERENCES

1 Jonas, D. M. Two-dimensional femtosecond spectroscopy. *Annu. Rev. Phys. Chem.* **2003**, *54*, 425–463.

2 Hochstrasser, R. M. Two-dimensional spectroscopy at infrared and optical frequencies. *Proc. Natl. Acad. Sci. U.S.A.* **2007**, *104*, 14190–14196.

3 Mukamel, S. *Principles of Nonlinear Optical Spectroscopy*; Oxford University Press: New York, 1995.

4 de Boeij, W. P.; Pshenichnikov, M. S.; Wiersma, D. A. Ultrafast solvation dynamics explored by femtosecond photon echo spectroscopies. *Annu. Rev. Phys. Chem.* **1998**, *49*, 99–123.

5 Renger, T.; May, V.; Kühn, O. Ultrafast excitation energy transfer dynamics in photosynthetic pigment−protein complexes. *Phys. Rep.* **2001**, *343*, 137–254.

6 Mukamel, S.; Abramavicius, D. Many-body approaches for simulating coherent nonlinear spectroscopies of electronic and vibrational excitons. *Chem. Rev.* **2004**, *104*, 2073–2098.

7 Bredenbeck, J.; Helbing, J.; Kolano, C.; Hamm, P. Ultrafast 2D-IR spectroscopy of transient species. *ChemPhysChem* **2007**, *8*, 1747–1756.

8 Zhuang, W.; Hayashi, T.; Mukamel, S. Coherent multidimensional vibrational spectroscopy of biomolecules: Concepts, simulations and challenges. *Angew. Chem.*, in print.

9 Cho, M. Coherent two-dimensional optical spectroscopy. *Chem. Rev.* **2008**, *108*, 1331–1418.

10 Dantus, M.; Lozovoy, V. V. Experimental coherent laser control of physicochemical processes. *Chem. Rev.* **2004**, *104*, 1813–1860.

11 Feynman, R. P. *Statistical Mechanics*; Addison−Wesley: London, U.K., 1972.

12 Gelin, M. F.; Pisliakov, A. V.; Egorova, D.; Domcke, W. A simple model for the calculation of nonlinear optical response functions and femtosecond time-resolved spectra. *J. Chem. Phys.* **2003**, *118*, 5287–5301.

13 Dellago, C.; Mukamel, S. Simulation algorithms for multidimensional nonlinear response of classical many-body systems. *J. Chem. Phys.* **2003**, *119*, 9344–9354.

14 Shi, Q.; Geva, E. A comparison between different semiclassical approximations for optical response functions in nonpolar liquid solution. II. The signature of excited state dynamics on two-dimensional spectra. *J. Chem. Phys.* **2008**, *129*, 124505.

15 Ishizaki, A.; Tanimura, Y. Modeling vibrational dephasing and energy relaxation of intramolecular anharmonic modes for multidimensional infrared spectroscopies. *J. Chem. Phys.* **2006**, *125*, 084501.

16 Gelin, M. F.; Egorova, D.; Domcke, W. Efficient method for the calculation of time- and frequency-resolved four-wave mixing signals and its application to photon-echo spectroscopy. *J. Chem. Phys.* **2005**, *123*, 164112.

17 Egorova, D.; Gelin, M. F.; Domcke, W. Analysis of cross peaks in two-dimensional electronic photon-echo spectroscopy for simple models with vibrations and dissipation. *J. Chem. Phys.* **2007**, *126*, 074314.

18 Seidner, L.; Stock, G.; Domcke, W. Nonperturbative approach to femtosecond spectroscopy: General theory and application to multidimensional nonadiabatic photoisomerization processes. *J. Chem. Phys.* **1995**, *103*, 3998–4011.

19 Wang, H.; Thoss, M. Nonperturbative quantum simulation of time-resolved nonlinear spectra: Methodology and application to electron transfer reactions in the condensed phase. *Chem. Phys.* **2008**, *347*, 139–151.

20 Meyer, S.; Engel, V. Non-perturbative wave-packet calculations of time-resolved four-wave-mixing signals. *Appl. Phys. B: Lasers Opt.* **2000**, *71*, 293–297.

21 Kato, T.; Tanimura, Y. Multi-dimensional vibrational spectroscopy measured from different phase-matching conditions. *Chem. Phys. Lett.* **2001**, *341*, 329–337.

22 Mancal, T.; Pisliakov, A. V.; Fleming, G. R. Two-dimensional optical three-pulse photon echo spectroscopy. I. Nonperturbative approach to the calculation of spectra. *J. Chem. Phys.* **2006**, *124*, 234504.

23 Kjellberg, P.; Pullerits, T. Three-pulse photon echo of an excitonic dimer modeled via Redfield theory. *J. Chem. Phys.* **2006**, *124*, 024106.

24 Cheng, Y. C.; Lee, H.; Fleming, G. R. Efficient simulation of three-pulse photon-echo signals with application to the determination of electronic coupling in a bacterial photosynthetic reaction center. *J. Phys. Chem. A* **2007**, *111*, 9499–9508.

25 Cheng, Y. C.; Engel, G. S.; Fleming, G. R. Elucidation of population and coherence dynamics using cross-peaks in two-dimensional electronic spectroscopy. *Chem. Phys.* **2007**, *341*, 285–295.

26 Cheng, Y. C.; Fleming, G. R. Coherence quantum beats in two-dimensional electronic spectroscopy. *J. Phys. Chem. A* **2008**, *112*, 4254–4260.

27 Egorova, D.; Gelin, M. F.; Domcke, W. Analysis of vibrational coherences in homodyne and two-dimensional heterodyne photon-echo spectra of Nile Blue. *Chem. Phys.* **2007**, *341*, 113–122.

28 Egorova, D. Detection of electronic and vibrational coherences in molecular systems by 2D electronic photon echo spectroscopy. *Chem. Phys.* **2008**, *347*, 166–176.

29 Weiss, U. *Quantum Dissipative Systems*; World Scientific: Singapore, 1999.

30 Tanimura, Y. Stochastic Liouville, Langevin, Fokker−Planck, and master equation approaches to quantum dissipative systems. *J. Phys. Soc. Jpn.* **2006**, *75*, 082001.

31 Egorova, D.; Gelin, M. F.; Thoss, M.; Wang, H.; Domcke, W. Effects of intense femtosecond pumping on ultrafast electronic−vibrational dynamics in molecular systems with relaxation. *J. Chem. Phys.* **2008**, *129*, 214303.

32 Pollard, W. T.; Felts, A. K.; Friesner, R. A. The Redfield equation in condensed-phase quantum dynamics. *Adv. Chem. Phys.* **1996**, *93*, 77–134.

33 Gelman, D.; Katz, G.; Kosloff, R.; Ratner, M. A. Dissipative dynamics of a system passing through a conical intersection: Ultrafast pump−probe observables. *J. Chem. Phys.* **2005**, *123*, 134112.

34 Brüggemann, B.; Persson, P.; Meyer, H.-D.; May, V. Frequency dispersed transient absorption spectra of dissolved perylene: A case study using the density matrix version of the MCTDH method. *Chem. Phys.* **2008**, *347*, 152–165.

35 Jansen, T. I. C.; Snijders, J. G.; Duppen, K. Interaction induced effects in the nonlinear Raman response of liquid CS2: A finite field nonequilibrium molecular dynamics approach. *J. Chem. Phys.* **2001**, *114*, 10910–10921.

36 DeVane, R.; Space, B.; Jansen, T. I. C.; Keyes, T. Time correlation function and finite field approaches to the calculation of the fifth order Raman response in liquid xenon. *J. Chem. Phys.* **2006**, *125*, 234501.

37 Saito, S.; Ohmine, I. Off-resonant two-dimensional fifth-order Raman spectroscopy of liquid CS2: Detection of anharmonic dynamics. *J. Chem. Phys.* **2003**, *119*, 9073–9087.

38 Yagasaki, T.; Saito, S. Ultrafast intermolecular dynamics of liquid water: A theoretical study on two-dimensional infrared spectroscopy. *J. Chem. Phys.* **2008**, *128*, 154521.

39 Hasegawa, T.; Tanimura, Y. Nonequilibrium molecular dynamics simulations with a backward−forward trajectories sampling for multidimensional infrared spectroscopy of molecular vibrational modes. *J. Chem. Phys.* **2008**, *128*, 064511.

40 Ka, B. J.; Geva, E. J. A nonperturbative calculation of nonlinear spectroscopic signals in liquid solution. *J. Chem. Phys.* **2006**, *125*, 214501.

41 Ding, F.; Zanni, M. T. Heterodyned 3D IR spectroscopy. *Chem. Phys.* **2007**, *341*, 95–105.

42 Hamm, P. Three-dimensional-IR spectroscopy: Beyond the two-point frequency fluctuation correlation function. *J. Chem. Phys.* **2006**, *124*, 124506.

43 Moran, A. M.; Park, S.; Scherer, N. F. Polarizability response spectroscopy: Formalism and simulation of ultrafast dynamics in solvation. *Chem. Phys.* **2007**, *341*, 344–356.

44 Zhang, Y.; Khadka, U.; Anderson, B.; Xiao, M. Temporal and spatial interference between four-wave mixing and six-wave mixing channels. *Phys. Rev. Lett.* **2009**, *102*, 013601.